

Cite this: *Phys. Chem. Chem. Phys.*, 2012, **14**, 15785–15792

www.rsc.org/pccp

PAPER

# $C_{2v}$ symmetrical two-photon polymerization initiators with anthracene core: synthesis, optical and initiating properties

Jin-Feng Xing,<sup>†a</sup> Mei-Ling Zheng,<sup>\*a</sup> Wei-Qiang Chen,<sup>a</sup> Xian-Zi Dong,<sup>a</sup>  
Nobuyuki Takeyasu,<sup>bc</sup> Takuo Tanaka,<sup>b</sup> Zhen-Sheng Zhao,<sup>a</sup> Xuan-Ming Duan<sup>\*a</sup>  
and Satoshi Kawata<sup>bcd</sup>

Received 23rd July 2012, Accepted 24th September 2012

DOI: 10.1039/c2cp42512b

A series of  $C_{2v}$  symmetrical two-photon absorption compounds with anthracene core, 2,7-bis[2-(4-substituted phenyl)-vinyl]-9,10-dipentyloxanthracenes designated as **I**, **II** and **III** (the substituted groups at the 4-position of phenyl of **I**, **II** and **III** were dimethylamino, methyl and cyano, respectively) were designed and synthesized as initiators in two-photon induced polymerization (TPIP). The anthracene ring was modified by linking vinylphenyl groups to the 2,7-position to extend conjugation system length and two pentyloxy groups to the 9,10-position to serve as electronic donors. Two-photon absorption cross section of **I** was around 300 GM, which was much larger than the 10 GM of **II** and 29 GM of **III** at 800 nm. **I** of 0.18% molar ratio in resin composed of methacrylic acid and dipentaerythritol hexaacrylate exhibited a dramatically low threshold of 0.64 mW compared with commercial photoinitiator benzil at a scanning speed  $10 \mu\text{m s}^{-1}$ . Moreover, the threshold of photoinitiator **I** was only increased to 2.53 mW at a scanning speed of  $1000 \mu\text{m s}^{-1}$ . The dependency of threshold on the concentration and exposure time was in accordance with theoretical calculation. Finally, a reasonable mechanism of the two-photon initiating process was proposed. This study provides good prospects for developing low threshold photoinitiator in TPIP.

## 1. Introduction

Two-photon induced polymerization (TPIP) has been one of the most attractive methods for three-dimensional (3D) lithography due to its intrinsic 3D fabrication capability and the nanometric resolution.<sup>1</sup> In the past decade, much progress in the TPIP lithography technique has been made in the resolution improvement and fabrication speed. Various kinds of complicated and functional 3D structures have been fabricated for potential applications.<sup>2</sup> In this fabrication technique, the most commonly used resins are the commercial negative-tone photoresist containing the conventional ultraviolet initiators

with low two-photon sensitivity due to their small two-photon absorption (TPA) cross sections ( $\delta_{\text{TPA}}$ ) at a few tens of GM ( $10^{-50} \text{ cm}^4 \text{ s photon}^{-1}$ ) level.<sup>3</sup> In general, the commercial resins cannot fulfil the increasing requirement for TPIP rapid microfabrication. Therefore, a highly sensitive TPIP initiator is required to achieve rapid TPIP microfabrication.

Varieties of novel compounds with large  $\delta_{\text{TPA}}$  have been designed as highly sensitive TPIP initiators.<sup>4</sup> Compounds with both large  $\delta_{\text{TPA}}$  and high initiating efficiency are required to achieve highly sensitive TPIP initiators. So far, the structure–property relations governing TPA have been studied extensively and many molecular design strategies were proposed to provide guidelines for the development of materials with large  $\delta_{\text{TPA}}$ . It has been confirmed that  $\delta_{\text{TPA}}$  increased with the donor/acceptor strength, conjugation length, molecular dimensionality and planarity of the  $\pi$ -center.<sup>5</sup> It is known that high initiating efficiency is also key for highly sensitive TPIP initiators besides large  $\delta_{\text{TPA}}$ . Naturally, optimizing conventional initiator systems to improve their  $\delta_{\text{TPA}}$  is a facile and efficient method to achieve highly sensitive TPIP initiators.<sup>6</sup>

The derivatives of anthracene have been widely used as UV photosensitizers or photoinitiators.<sup>7</sup> Recently, the utility of the anthracene as a special and efficient  $\pi$ -center for the two-photon chromophores has been demonstrated by several research groups.<sup>8</sup> The good co-planarity of anthracene could contribute to the improvement of  $\delta_{\text{TPA}}$ .<sup>9</sup> Basically, the anthracene unit

<sup>a</sup> Laboratory of Organic NanoPhotonics and Key Laboratory of Functional Crystals and Laser Technology, Technical Institute of Physics and Chemistry, Chinese Academy of Sciences, No. 29, Zhongguancun East Road, Beijing 100190, P. R. China.  
E-mail: zhengmelling@mail.ipc.ac.cn, xmduan@mail.ipc.ac.cn;  
Fax: +86-10-82543597; Tel: +86-10-82543596

<sup>b</sup> Nanophotonics Laboratory RIKEN (The Institute of Physical and Chemical Research), 2-1 Hirosawa, Wako, Saitama 351-0198, Japan

<sup>c</sup> Photonics Center, Osaka University, 2-1 Yamadaoka, Suita Osaka 565-0871, Japan

<sup>d</sup> Department of Applied Physics, Osaka University, 2-1 Yamadaoka, Suita Osaka 565-0871, Japan

<sup>†</sup> Present address: Department of Polymer Science and Engineering, School of Chemical Engineering and Technology, Tianjin University, Tianjin 300072, China.

could be linked to 9,10-, 2,6- and 2,7-linkages to form three different conjugation pathways with different quinoid characters. Among those three types of anthracene derivatives, 9,10- and 2,6-linkages were widely synthesized and studied due to their high fluorescence quantum yield and large  $\delta_{\text{TPA}}$ . Those two types of anthracene derivatives have potential applications in the investigation of two-photon excited fluorescence (TPEF) and photo-induced electron transfer. However, the study on 2,7-linkage type anthracene derivatives with  $C_{2v}$  symmetrical conjugated system has been ignored. So far, only one 2,7-linkage type anthracene derivative, 2,7-bis(4-dihexylamino-styryl)-9,10-dicyanoanthracene, has been synthesized and investigated. It possessed much lower fluorescence quantum yield ( $\Phi_{\text{fl}}$ ) compared with its linear analog, 2,6-bis(4-dihexylaminostyryl)-9,10-dicyanoanthracene.<sup>9</sup> Considering the competition in the relaxation processes of the excited state, it is clear that a lower  $\Phi_{\text{fl}}$  is favorable to achieve higher initiating efficiency for photopolymerization, since the proportion of relaxation through non-irradiation processes would increase in this case. Our previous work also demonstrated that chromophores with  $C_{2v}$  symmetrical conjugated systems possessed dramatically low  $\Phi_{\text{fl}}$  and presented good TPIP initiating properties.<sup>10</sup>

In this study, we focused on designing and synthesizing a series of 2,7-bis[2-(4-substituted phenyl)-vinyl]-9,10-dipentyl-oxanthracenes, **I**, **II** and **III** (the substituted groups at 4-position of phenyl for **I**, **II** and **III** are dimethylamino, methyl and cyano groups, respectively) with  $C_{2v}$  symmetry structure through the Wittig reaction. We modified the anthracene ring by linking vinylphenyl groups to the 2,7-position instead of the 2,6-position by reducing the symmetry of TPA molecules to avoid the high  $\Phi_{\text{fl}}$ . The modification of the 2,7-position in the anthracene ring with vinylphenyl groups resulted in a large conjugation system with  $C_{2v}$  symmetry. The substituents at the 4-position of benzene of the vinylphenyl moieties worked as electronic donor or acceptor according to their electron-donating capability. Two pentyloxy groups at the 9,10-position of the anthracene ring served as electronic donors and played an important role in the solubility improvement in resin. These anthracene derivatives with a large conjugation system would improve the  $\pi$ -conjugated intramolecular charge transfer (ICT), and their  $C_{2v}$  symmetric structures would reduce the symmetry of these molecules and lead to a lower  $\Phi_{\text{fl}}$ . This concept of molecular design could contribute to a large  $\delta_{\text{TPA}}$  and high TPIP initiating activities. The one-photon absorption and two-photon absorption properties as well as TPIP initiating properties of these compounds have been investigated, and the TPA initiating mechanism of 9,10-dialkoxyanthracene has been proposed.

## 2. Experimental section

### 2.1 Materials and characterization

*N*-bromosuccinimide (NBS), benzoyl peroxide (BPO), toluene, anhydrous sodium acetate, acetic acid, acetic anhydride, methanol, sodium hydroxide (NaOH), tetrabutyl ammonium bromide (TBAB), tetrahydrofuran (THF), thionyl chloride, sodium dithionite ( $\text{Na}_2\text{S}_2\text{O}_4$ ), 1-bromo-pentane, chloroform ( $\text{CHCl}_3$ ), chloroform- $D$  ( $\text{CDCl}_3$ ), anhydrous magnesium

sulfate ( $\text{MgSO}_4$ ), petroleum ether, ethyl acetate, triphenyl phosphine ( $\text{PPh}_3$ ), sodium hydride (NaH), methacrylic acid (MA) and benzil were of reagent grade and purchased from Beijing Chemical Reagent Company. Dichloromethane ( $\text{CH}_2\text{Cl}_2$ , spectrophotometric grade) was also obtained from Beijing Chemical Reagent Company. 4-Dimethylamino-benzaldehyde, 4-methylbenzaldehyde, 4-cyanobenzaldehyde and 2-methyl phthalic anhydride were obtained from J&K Chemicals Company. Dipentaerythritol hexaacrylate (DPE-6A, trade name: light acrylate DPE-6A) was purchased from Kyoisha Chemical Co., Ltd., Japan. Silica gel (200–300 mesh, Beijing Chemical Reagent Company) was used in column chromatography as the stationary phase. The  $^1\text{H}$  NMR spectra were recorded on a Varian-300 or Bruker AMX-400. Infrared spectra were recorded on a FTIR-410 spectrophotometer (JASCO Corp.) in the range 4000–400  $\text{cm}^{-1}$  with a resolution of 1.0  $\text{cm}^{-1}$ . High resolution mass spectra (HRMS) were recorded on a JEOL JMS-700 instrument.

### 2.2 Measurements

The UV-vis absorption spectra were recorded on UV-2550 Shimadzu UV-vis spectrophotometer at a concentration of  $1 \times 10^{-5}$  M in  $\text{CH}_2\text{Cl}_2$  and fluorescence spectra were recorded on a Hitachi F-4500 fluorescence spectrophotometer at a concentration of  $1 \times 10^{-6}$  M in  $\text{CH}_2\text{Cl}_2$ . The fluorescence quantum yields were measured using coumarin 307 in acetonitrile as reference standard ( $\Phi_{\text{fl}} = 0.58$ ).<sup>11</sup> The one-photon excited fluorescence (OPEF) lifetimes were measured using a streak scope camera (Hamamatsu, C4334) with the excitation of femtosecond laser pulse at 400 nm. The time resolution of the system was limited by that of the streak camera of about 10 ps. TPEF spectra were recorded on SD2000 spectrometer (Ocean Optics) at a concentration of  $1 \times 10^{-4}$  M in  $\text{CH}_2\text{Cl}_2$  with excitation by using a femtosecond laser (Tsunami, Spectra-Physics) with a pulse width of 80 fs and repetition rate of 80 MHz.  $\delta_{\text{TPA}}$  was determined by the two-photon induced fluorescence method.<sup>12</sup>

### 2.3 Synthesis and characterization of compounds

**2,7-Dibromomethyl-anthraquinone (B).** 2,7-Dimethyl-anthraquinone (5.834 g, 24.6 mmol) and NBS (11.413 g, 64.1 mmol) were added to a three-necked flask containing  $\text{CCl}_4$  (400.0 mL). After the suspension was heated to 70  $^\circ\text{C}$ , benzoyl peroxide (0.760 g, 3.30 mmol) was added. Then, the suspension was heated at reflux for 24 h. When the mixture was cooled down to room temperature, the precipitate was filtered, washed with water (200.0 mL  $\times$  3), dried under vacuum, and recrystallized from toluene to give **B** (5.838 g, 60%) as a light yellow solid. Mp 271–273  $^\circ\text{C}$ ;  $\delta_{\text{H}}$  (300 MHz,  $\text{CDCl}_3$ ): 8.33 (s, 2H), 8.30 (d,  $J = 8.1$  Hz, 2H), 7.83 (d,  $J = 8.1$  Hz, 2H), 4.60 (s, 4H).

**2,7-Diacetoxymethyl-9,10-anthraquinone (C).** 2,7-Dibromomethyl-anthraquinone (4.030 g, 10.2 mmol) was added into a solution of anhydrous sodium acetate (11.893 g, 145 mmol) in acetic acid (60.0 mL) and acetic anhydride (60.0 mL). The mixture was heated at reflux for 14 h. Then, the solvent was removed by distillation. The residue was cooled down and poured into water. The precipitate was collected and washed with water until the acid was free. The crude product was

purified by recrystallization from toluene to give **C** (2.000 g, 58%) as a white solid. Mp 145–146 °C;  $\delta_{\text{H}}$  (300 MHz,  $\text{CDCl}_3$ ) 8.21 (d,  $J = 7.8$  Hz, 2H), 8.17 (s, 2H), 7.90 (d,  $J = 7.8$  Hz, 2H), 5.28 (s, 4H), 2.15 (s, 6H).

**2,7-Dihydroxymethyl-9,10-anthraquinone (D).** 2,7-Diacetoxymethyl-9,10-anthraquinone (0.102 g, 0.28 mmol) was added to methanol (15.0 mL), then the solution of NaOH (0.050 g, 1.25 mmol) in water (5.0 mL) was added. The mixture was heated at reflux for 17 h. After the mixture was cooled down to room temperature, it was poured into water. The precipitate was collected and dried in vacuum. The crude product was dissolved into chloroform and purified by silica gel chromatography (eluent: petroleum ether and ethyl acetate) to give **D** (0.040 g, 53%) as a white solid. Mp 203–205 °C;  $\delta_{\text{H}}$  (300 MHz,  $\text{CDCl}_3$ ) 8.17 (s, 4H), 7.85 (d,  $J = 8.0$  Hz, 2H), 5.59 (s, 2H), 4.70 (s, 4H).

**2,7-Dihydroxymethyl-9,10-dipentyloxy-anthracene (E).** 2,7-Dihydroxymethyl-9,10-anthraquinone (0.206 g, 0.76 mmol) and TBAB (0.241 g, 0.74 mmol) were dissolved in THF (15.0 mL) and water (15.0 mL), and stirred at room temperature, followed by the addition of a solution of sodium dithionite (0.529 g, 3.04 mmol) in water (10.0 mL). After 10 min, a solution of NaOH (0.744 g, 18.6 mmol) in water (3.0 mL) was added. The reaction mixture immediately turned into dark red. 1-Bromopentane (2.0 mL) was added and the reaction mixture was heated at reflux for 30 h. After the mixture was cooled down to room temperature, the mixture was extracted with chloroform (15.0 mL  $\times$  3). The extract was washed with water and dried over anhydrous  $\text{MgSO}_4$ . After filtration, the filtrate was concentrated. The crude product was purified by silica gel chromatography (eluent: petroleum ether and ethyl acetate) to give **E** (0.140 g, 47%) as a light yellow solid. Mp 131–133 °C;  $\delta_{\text{H}}$  (300 MHz,  $\text{CDCl}_3$ ) 8.35–8.19 (m, 4H), 7.54 (t, 2H), 4.92 (s, 4H), 4.15 (t, 2H), 3.53 (t, 2H), 2.06 (s, 2H), 1.81 (m, 4H), 1.53 (m, 8H), 1.03 (m, 6H).

**2,7-Dichloromethyl-9,10-dipentyloxy-anthracene (F).** 2,7-Dihydroxymethyl-9,10-dipentyloxy-anthracene (0.908 g, 2.21 mmol) was dissolved in dry  $\text{CHCl}_3$  (35.0 mL). The solution was cooled to below 5 °C. A solution of thionyl chloride (14.400 g, 121 mmol) in  $\text{CHCl}_3$  (10.0 mL) was added. The reaction mixture was stirred at room temperature for 3 h. The mixture was washed with water, and dried over anhydrous  $\text{MgSO}_4$ . The filtrate was concentrated and the residue was purified by silica gel chromatography (eluent: petroleum ether and ethyl acetate) to give **F** (0.520 g, 72%) as a light yellow solid. Mp 75–77 °C;  $\delta_{\text{H}}$  (300 MHz,  $\text{CDCl}_3$ ) 8.27 (d,  $J = 8.8$  Hz, 2H), 8.23 (s, 2H), 7.50 (d,  $J = 8.8$  Hz, 2H), 4.82 (s, 4H), 4.15 (m, 4H), 2.07 (m, 4H), 1.62 (m, 4H), 1.47 (m, 4H), 1.00 (m, 6H).

**2,7-Bis(triphenylphosphonium)-9,10-dipentyloxy-anthracene dichloride (G).** 2,7-Dichloromethyl-9,10-dipentyloxy-anthracene (0.198 g, 0.44 mmol) and  $\text{PPh}_3$  (1.08 g, 4.12 mmol) were dissolved in toluene (40.0 mL). The reaction mixture was heated at reflux for 24 h. Then, the precipitate was filtered, washed with toluene (2.0 mL  $\times$  3) and dried in vacuum to give **G** (0.208 g, 72%) as a yellow solid. Mp > 300 °C;  $\delta_{\text{H}}$  (300 MHz,  $\text{CDCl}_3$ ) 7.93–7.61 (m, 36H), 3.95 (t,  $J = 6.7$  Hz, 4H), 3.40 (m, 4H), 1.90 (m, 4H), 1.42 (m, 4H), 0.99 (m, 6H).

**2,7-Bis[2-(4-dimethylamino-phenyl)vinyl]-9,10-dipentyloxy-anthracene (I).** 2,7-Bis(triphenylphosphonium)-9,10-dipentyloxy-anthracene (0.308 g, 0.31 mmol) and 4-dimethylamino-benzaldehyde (0.093 g, 0.06 mmol) were added to a two-necked flask containing absolute THF (40.0 mL) under  $\text{N}_2$ , then NaH (0.140 g, 5.83 mmol) was added into the mixture. The reaction mixture was allowed to reflux for 15 h. Water (20.0 mL) was added slowly after the solution was cooled to room temperature. The mixture was extracted with chloroform (20.0 mL  $\times$  3). The combined extract was washed with water (10.0 mL  $\times$  2) and dried over anhydrous  $\text{MgSO}_4$ . After filtration, the filtrate was concentrated and purified by silica gel chromatography (eluent: petroleum ether and ethyl acetate) to give **I** (0.080 g, 40%) as a yellow solid.  $\delta_{\text{H}}$  (400 MHz,  $\text{CDCl}_3$ ) 8.14 (m, 4H), 7.67 (m, 2H), 7.44 (d,  $J = 10.6$  Hz, 4H), 7.12 (m, 8H), 6.69 (d,  $J = 10.6$  Hz, 4H), 4.11 (m, 4H), 3.41 (s, 4H), 2.94 (m, 12H), 2.10 (m, 4H), 1.65 (m, 4H), 1.46–1.19 (m, 8H), 1.01–0.81 (m, 6H); HRMS: calcd for  $\text{C}_{44}\text{H}_{52}\text{N}_2\text{O}_2$ : 640.4029, found: 640.3991 (–5.9 ppm).

**2,7-Bis-[2-(*p*-tolyl)-vinyl]-9,10-dipentyloxy-anthracene (II).** Synthesized by the same procedure as for **I**; yellow solid, yield 65%.  $\delta_{\text{H}}$  (400 MHz,  $\text{CDCl}_3$ ) 8.21 (m, 4H), 7.78 (m, 2H), 7.90 (d,  $J = 8.1$  Hz, 4H); 7.22 (m, 4H), 6.95 (d,  $J = 8.1$  Hz, 4H), 4.18 (m, 4H), 3.85 (s, 6H), 3.50 (m, 4H), 2.10 (m, 4H), 1.80 (m, 4H), 1.7 (m, 4H), 1.56 (m, 4H), 1.51 (m, 4H), 1.30 (m, 4H), 1.03 (m, 6H), 0.97 (m, 6H); HRMS: calcd for  $\text{C}_{42}\text{H}_{46}\text{O}_2$ : 582.3498, found: 582.3477 (–3.6 ppm).

**2,7-Bis[2-(4-cyanophenyl)vinyl]-9,10-dipentyloxy-anthracene (III).** Synthesized by the same procedure as for **I**; orange solid, yield 42%.  $\delta_{\text{H}}$  (400 MHz,  $\text{CDCl}_3$ ) 8.41 (m, 2H), 8.32 (m, 2H), 7.91 (m, 2H), 7.86–7.35 (m, 12H), 4.21 (m, 4H), 3.01 (s, 4H), 2.14 (m, 4H), 1.80 (m, 4H), 1.71–1.20 (m, 8H), 1.05 (m, 6H), 0.80 (m, 6H); HRMS: calcd for  $\text{C}_{42}\text{H}_{40}\text{N}_2\text{O}_2$ : 604.3090, found: 604.3087 (–0.5 ppm).

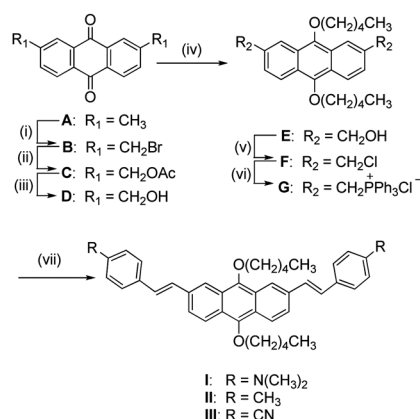
## 2.4 Two-photon induced polymerization

TPIP experiments were performed by resins exposed in the pattern of a target structure with a tightly focused (60 $\times$  /1.42 NA oil immersion objectives) laser pulse from a Ti:sapphire laser with a wavelength of 800 nm, pulse width of 80 fs and repetition rate of 80 MHz. The resins were prepared by mixing the monomer and photoinitiator. For example, MA (102.0 mg, 66.47 wt% in resin), multifunctional acrylic compound DPE-6A (50.0 mg, 32.59 wt% in resin) as crosslinker, **I** (1.45 mg, 0.94 wt% or 0.18 mol% in resin) and THF (0.1 mL) were mixed to give resin 1 (**R**<sup>1</sup>). Resins 2–8 (**R**<sup>2</sup>–**R**<sup>8</sup>) were prepared in the same way. The exposure time was controlled by a shutter. Final structures were obtained after development using ethanol. The images of fabricated lines were observed using a field-emission scanning electron microscope (FE-SEM, JOEL, JSM-6330F). The working voltage and current were 5 kV and 8  $\mu\text{A}$ , respectively.

## 3. Results and discussion

### 3.1 Synthesis of designated anthracene derivatives

2,7-Dimethyl-anthraquinone (**A**) was prepared from 2-methyl phthalic anhydride according to reference 13 in two steps. Starting from 2,7-dibromomethyl-anthraquinone (**B**), compound **D**



**Scheme 1** Synthetic route for **I–III**. Reagents and conditions: (i) NBS/BPO/CCl<sub>4</sub>, 60%; (ii) anhydrous sodium acetate/acetic acid/acetic anhydride, 58%; (iii) NaOH/methanol/H<sub>2</sub>O, 53%; (iv) Na<sub>2</sub>S<sub>2</sub>O<sub>4</sub>/NaOH/TBAB/CH<sub>3</sub>(CH<sub>2</sub>)<sub>4</sub>Br/H<sub>2</sub>O/THF, 47%; (v) thionyl chloride/CHCl<sub>3</sub>, 72%; (vi) PPh<sub>3</sub>/toluene, 72%; (vii) *p*-R-C<sub>6</sub>H<sub>4</sub>CHO/NaH/THF, 40–65%.

was prepared after esterification and deprotection. Then, the quinone moiety of **D** was reduced and protected by a pentyloxy group. **E** reacted with thionyl chloride followed by the treatment of triphenylphosphine to give the salt **G**. Further Wittig reaction gave compounds **I–III** (Scheme 1).

### 3.2 Linear optical properties

The normalized one-photon absorption and fluorescence spectra in CH<sub>2</sub>Cl<sub>2</sub> of **I–III** were shown in Fig. 1a and Fig. 1b, respectively. The results of the photophysical measurements were

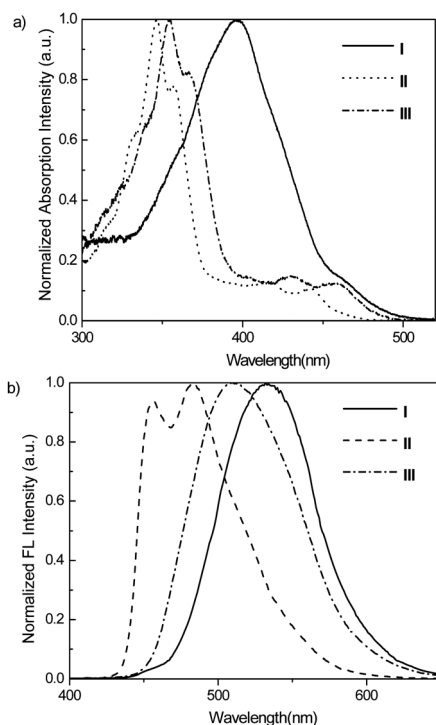


**Fig. 1** (a) Normalized UV-vis spectra of **I** (solid), **II** (dot) and **III** (dash dot) in CH<sub>2</sub>Cl<sub>2</sub>; (b) Normalized fluorescence spectra of **I** (solid), **II** (dot) and **III** (dash dot) in CH<sub>2</sub>Cl<sub>2</sub> obtained at the excitation wavelength of 400 nm.

**Table 1** The photophysical properties of **I–III** in CH<sub>2</sub>Cl<sub>2</sub> at 25 °C<sup>a</sup>

	$\lambda_{\max}^{(1)}$	$\lambda_{\max}^{(\text{OPF})}$	ST	$\Phi_{\text{fl}}$	$\tau$ (ns)	$\lambda_{\max}^{(\text{TPF})}$	$\lambda_{\max}^{(2)}$	$\delta_{\max}$
<b>I</b>	396	532	136	0.17	3.46 ± 0.16	538	750	466
<b>II</b>	347	484	137	0.36	2.79 ± 0.11	490	700	78
<b>III</b>	355	510	155	0.22	3.24 ± 0.05	524	700	121

<sup>a</sup>  $\lambda_{\max}^{(1)}$  is the one-photon absorption maximum.  $\lambda_{\max}^{(\text{OPF})}$  is the wavelength of one-photon fluorescence peak.  $\Phi_{\text{fl}}$  is fluorescence quantum yield. ST is the Stokes shift; ST = ( $\lambda_{\max}^{(\text{OPF})}$ ) - ( $\lambda_{\max}^{(1)}$ ).  $\tau$  is fluorescence lifetime excited at a wavelength of 400 nm.  $\lambda_{\max}^{(\text{TPF})}$  is the wavelength of two-photon fluorescence peak.  $\lambda_{\max}^{(2)}$  is the wavelength of TPA maximum.  $\delta_{\max}$  is the maximum value of TPA cross section. 1 GM = 10<sup>-50</sup> cm<sup>4</sup> s photon<sup>-1</sup>.

summarized in Table 1. The absorption maximum appeared at 396 nm for **I**, 347 nm for **II** and 355 nm for **III**, respectively. The absorption band showed a red-shift of around 40 nm when a strong electron-donating (**I**) end group was used, indicating an enlargement of the ICT extent.<sup>14</sup> According to reference 9, it is known that two-photon allowed states for quadrupoles are at a higher energy than the Frank–Condon states. For the end groups with weak electron-donating (**II**) or electron-withdrawing (**III**) strength, although the absorption maximum is shorter than 360 nm, there are several peaks in the absorption spectra. This indicates an increased number of one-photon-allowed states, demonstrating that the structures of **II** and **III** are probably distorted and the ICT is significantly inhibited, which would in turn increase the probability of the localized absorption.<sup>15</sup>

The fluorescence emission spectra (Fig. 1b) of **II** showed two emission peaks with a maximum at 484 nm and another at 458 nm, indicating the existence of more than one emitting state.<sup>15</sup> There was a large Stokes shift for these three compounds (Table 1). Compared to **II**, the emission bands of **I** and **III** was red-shifted 48 nm and 26 nm, respectively. This result indicated that molecules typically underwent a large change in dipole moment upon electronic excitation.<sup>16</sup> None of the fluorescence spectra of **I** and **III** have multiple peaks, which indicates that the emission occurs from the lowest excited state.<sup>9</sup> Fluorescence is a process competing with other deactivation pathways like intersystem crossing from singlet excited state (S<sub>1</sub>) to the lowest triplet state (T<sub>1</sub>). It was extensively demonstrated that the main route of most photoreaction occurs *via* the T<sub>1</sub> level which is related to the efficiency of photoinitiator as it leads to bond breaking and the formation of radicals.<sup>17</sup> Thus, it can be assumed that high  $\Phi_{\text{fl}}$  is indicative of low efficiency in radical formation. The  $\Phi_{\text{fl}}$  of **II** was more than twice as high as that of **I** (Table 1), indicating a lower efficiency of **II** in radical formation. The shorter fluorescence lifetime of **II** compared with **I** also implies that the C<sub>2v</sub> symmetric chromophores with strong donors are advantageous to improve the efficiency of radical formation. The lower  $\Phi_{\text{fl}}$  and longer fluorescence lifetime for **I** and **III** were attributed to dominant nonradiative decay mechanisms.<sup>18</sup> The irradiative decay constants ( $k_{\text{r}}$ ,  $k_{\text{r}} = \Phi_{\text{fl}}/\tau$ ) of **I**, **II** and **III** are  $4.91 \times 10^7 \text{ s}^{-1}$ ,  $1.29 \times 10^8 \text{ s}^{-1}$  and  $6.79 \times 10^7 \text{ s}^{-1}$ , respectively. The nonradiative decay constant ( $k_{\text{nr}}$ ) can be calculated from  $k_{\text{r}}$  and  $\Phi_{\text{fl}}$  according to the equation:<sup>19</sup>

$$k_{\text{nr}} = \left( \frac{1}{\Phi_{\text{fl}}} - 1 \right) k_{\text{r}}$$

The  $k_{nr}$  of **I**, **II** and **III** are  $2.40 \times 10^8 \text{ s}^{-1}$ ,  $2.29 \times 10^8 \text{ s}^{-1}$  and  $2.41 \times 10^8 \text{ s}^{-1}$ , respectively. Therefore, the nonradiative decay of **I** and **III** are faster than that of **II**.

### 3.3 TPA property

The two-photon fluorescence spectra of **I–III** were obtained at the excitation wavelength of 800 nm and the emission maxima appeared at wavelengths ranging from 491 to 538 nm (Fig. 2a). The maxima in the two-photon fluorescence spectra of **I–III** showed slight red-shift compared to their one-photon fluorescence spectra. It is well known that two-photon excitation process induces different excited states for molecules compared with single photon excitation, and the different excited states by one- and two-photon absorption leads to the differences in relaxing and emitting processes.<sup>20</sup>

To demonstrate the applicability of the molecules designed for TPIP, we have evaluated the  $\delta_{\text{TPA}}$  of compounds **I–III** in the range of 700–880 nm. The two-photon absorption spectra of **I–III** were shown in Fig. 2b. The values of  $\delta_{\text{max}}$  in the range of 700–880 nm were listed in Table 1. The largest value of  $\delta_{\text{TPA}}$  obtained was 466 GM for **I** at 750 nm, which was much larger than those of **II** and **III**. The enhancement of  $\delta_{\text{TPA}}$  for **I** compared with those of **II** and **III** was mainly attributed to the contribution from the strong electronic donating capability of dimethylamino groups at the 4-position of benzene rings, since the strong electronic donors led to large ICT. The value of  $\delta_{\text{TPA}}$  for **I** at 800 nm, the mostly used wavelength in TPIP microfabrication, remained at a high level of around 300 GM, which was much larger than those of the commercial photoinitiators.<sup>3</sup> It indicates that the resin using **I** as photoinitiator may exhibit higher two-photon photosensitivity.

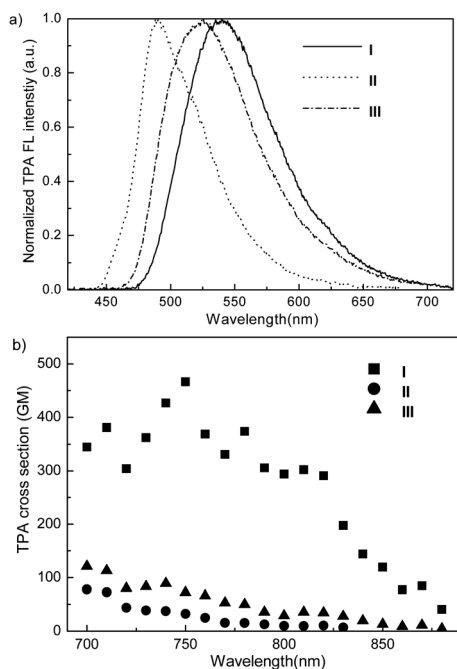


**Fig. 2** (a) Normalized two-photon fluorescence spectra of **I–III** in  $\text{CH}_2\text{Cl}_2$ ; (b) two-photon absorption spectra of **I–III** in  $\text{CH}_2\text{Cl}_2$ .

### 3.4 Two-photon induced polymerization

The threshold energy of TPIP is one of the most effective parameters to evaluate initiating efficiency of a photoinitiator. Usually, the threshold energy of TPIP is defined as the lowest average laser power which can produce the solid polymer lines from a photoresist resin.<sup>21</sup> Considering the fact that photoresist resins usually contain monomers and crosslinkers, the polymer after photopolymerization is supposed to be a single huge polymer molecule including a network. The threshold energy of TPIP means the lowest laser power which can generate enough radicals for constructing a polymer network, and still has the resistance to not develop. The capability for forming polymer network is influenced by many factors, such as the components of monomers, crosslinkers, photoinitiators, and laser exposure parameters.

Here, we focus our investigation on the evaluation of the initiating efficiencies of photoinitiators based on the discussion of TPIP mechanism. The polymerization threshold ( $P_{\text{th}}$ ) is defined as the average power before the objective lens, below which the polymer line cannot be fabricated using a linear scanning speed of  $10 \mu\text{m s}^{-1}$ . Therefore, the TPIP threshold of exposure intensity ( $E_{\text{th}}$ ) can be calculated as the lowest laser intensity. In order to evaluate the TPIP initiating efficiency of **I–III** in the aspects of threshold intensity, we have designed three experimental samples including (1) resins designated as **R<sup>1</sup>**, **R<sup>2</sup>**, **R<sup>3</sup>** and **R<sup>4</sup>** containing the same molar ratio of **I–III** and benzil at a fixed laser scanning speed of  $10 \mu\text{m s}^{-1}$ , respectively; (2) resins designated as **R<sup>1</sup>**, **R<sup>5</sup>**, **R<sup>6</sup>**, **R<sup>7</sup>** and **R<sup>8</sup>** containing different molar ratio of **I** at a fixed laser scanning speed of  $10 \mu\text{m s}^{-1}$ , respectively, and (3) **R<sup>1</sup>** containing 0.18% molar ratio of **I** at different laser scanning speeds. The components and polymerization threshold of **R<sup>1–4</sup>** are summarized in Table 2. The SEM images on the TPIP results of **R<sup>1–4</sup>** are shown in Fig. 3. The  $P_{\text{th}}$  for **R<sup>1</sup>**, **R<sup>2</sup>**, **R<sup>3</sup>** and **R<sup>4</sup>** at a linear scanning speed of  $10 \mu\text{m s}^{-1}$  were 0.64, 1.60, 8.37 and 6.37 mW, respectively. As we know, polymerization rate can be denoted by number of monomer changing into polymer per second. Polymer volume per second is enlarged when the monomers change into polymer per second. Therefore, polymer volume per second can be used to express the polymerization rate indirectly. Polymer volume per second of TPIP ( $R_p$ ) can be calculated by the equation  $R_p = \pi(d/2)^2\nu_s$ , where  $d$  is the width of fabricated line and  $\nu_s$  is linear scanning speed.<sup>21</sup> As shown in Fig. 4, the results show that the sensitivity of resins is **R<sup>1</sup>** > **R<sup>2</sup>** > **R<sup>4</sup>** > **R<sup>3</sup>**, corresponding to the photoinitiating efficiency of compounds that is **I** > **II** > benzil > **III**. According to the reference, the

**Table 2** TPIP threshold of resins

MA (wt%)	DPE-6A (wt%)	MR <sup>a</sup> (%)	$\nu_s^b$ ( $\mu\text{m s}^{-1}$ )	$P_{\text{th}}^c$ (mW)	$E_{\text{th}}^d$ ( $\text{mJ cm}^{-2}$ )
<b>R<sup>1</sup></b> 66.47	32.59	0.18	10	0.64	$2.77 \times 10^7$
<b>R<sup>2</sup></b> 66.53	32.61	0.18	10	1.60	$6.93 \times 10^7$
<b>R<sup>3</sup></b> 66.50	32.61	0.18	10	8.37	$3.56 \times 10^8$
<b>R<sup>4</sup></b> 66.89	32.80	0.18	10	6.37	$2.82 \times 10^8$

<sup>a</sup> Molar ratio of initiator in resin. <sup>b</sup> Linear scanning speed. <sup>c</sup> Threshold power of dye in resin. <sup>d</sup> Exposure intensity at threshold power.

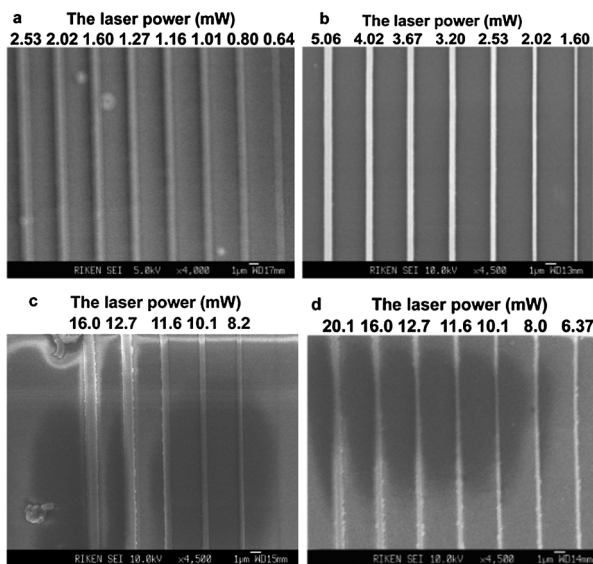


**Fig. 3** SEM images of **R**<sup>1</sup> (a), **R**<sup>2</sup> (b), **R**<sup>3</sup> (c) and **R**<sup>4</sup> (d) after TPIP, respectively. The linear scanning speed was 10  $\mu\text{m s}^{-1}$ .

amount of photogenerated radicals can be expressed with the following equation:<sup>22</sup>

$$[A_c] = \Phi \frac{\delta_{\text{TPA}}}{2(h\nu)^2} [A] \int I_{\text{pulse}}^2 dt \times N_{\text{pulse}}$$

where,  $\Phi$  is quantum efficiency of radical generation, and  $[A]$  is the concentration of the photoinitiator.  $I$ ,  $h\nu$  and  $N_{\text{pulse}}$  are the pulse intensity, photon energy and the number of pulses, respectively.

If the solidified polymer formed at the threshold was treated as a molecule and its formation only depended on the amount of photogenerated radicals, the photoinitiator initiating efficiency would depend on  $\delta_{\text{TPA}}$  and  $\Phi$ . Therefore, the larger  $\delta_{\text{TPA}}$  at 800 nm and lower  $\Phi_{\text{fl}}$  of **I** contributed to the higher sensitivity of **R**<sup>1</sup> compared with those of **II** and **III**. This result can be attributed to the stronger electron donating ability of dimethylamino group in **I** compared with methyl group in **II** and cyano group in **III**, which would stabilize radicals produced by two-photon excitation.<sup>23</sup> The threshold exposure intensity  $E_{\text{th}}$  of **R**<sup>1</sup> was  $2.77 \times 10^7 \text{ mJ cm}^{-2}$ , which was ten times lower than  $2.82 \times 10^8 \text{ mJ cm}^{-2}$  for **R**<sup>4</sup> that used benzil as photoinitiator. The polymerization rate of **R**<sup>1</sup> was

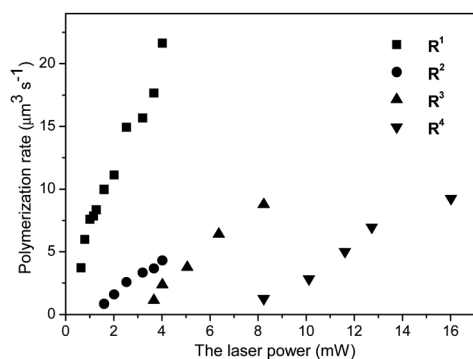


**Fig. 4** TPIP rates of **R**<sup>1</sup>, **R**<sup>2</sup>, **R**<sup>3</sup> and **R**<sup>4</sup>, respectively. The linear scanning speed was 10  $\mu\text{m s}^{-1}$ .

**Table 3** TPIP threshold resins with different concentrations

	MA (wt%)	DPE-6A (wt%)	MR <sup>a</sup> (%)	$\nu_s^b$ ( $\mu\text{m s}^{-1}$ )	$P_{\text{th}}^c$ (mW)	$E_{\text{th}}^d$ ( $\text{mJ cm}^{-2}$ )
<b>R</b> <sup>1</sup>	66.47	32.59	0.18	10	0.64	$2.77 \times 10^7$
<b>R</b> <sup>5</sup>	66.78	32.75	0.09	10	1.01	$4.37 \times 10^7$
<b>R</b> <sup>6</sup>	66.94	32.82	0.045	10	1.60	$6.93 \times 10^7$
<b>R</b> <sup>7</sup>	67.02	32.86	0.023	10	2.02	$8.74 \times 10^7$
<b>R</b> <sup>8</sup>	67.06	32.88	0.012	10	5.06	$2.19 \times 10^8$

<sup>a</sup> Molar ratio of initiator in resin. <sup>b</sup> Linear scanning speed. <sup>c</sup> Threshold power of dye in resin. <sup>d</sup> Exposure intensity at threshold power.

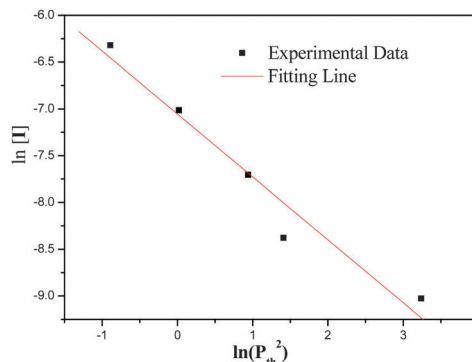
much larger than that of **R**<sup>4</sup>, demonstrating that resin **R**<sup>1</sup> with **I** as two-photon photoinitiator exhibited much higher sensitivity than benzil.

High initiating efficiency of **I** encouraged us to further investigate its initiating property with lower loading in resin. The components and TPIP threshold of **R**<sup>1</sup> and **R**<sup>5</sup>–**R**<sup>8</sup> are summarized in Table 3. When the molar ratio of **I** was reduced from 0.18% in resin **R**<sup>1</sup> to 0.012% in resin **R**<sup>8</sup>, the threshold power increased from 0.64 to 5.06 mW. Correspondingly, the threshold laser exposure intensity increased from  $2.77 \times 10^7$  to  $2.19 \times 10^8 \text{ mJ cm}^{-2}$ . The dependence of threshold power  $P_{\text{th}}^2$  on the concentration of **I** was shown in Fig. 5. There is a relationship as shown in the equation:

$$\ln(P_{\text{th}}^2) = \ln N - \ln[I]$$

where,  $P_{\text{th}}$  is the threshold laser power,  $[I]$  is the molar ratio of the photoinitiator **I** in resin, here  $N$  is considered to be constant decided by  $\delta_{\text{TPA}}$ , the quantum yield of radical generation and the exposure time. According to this equation, when the concentration of photoinitiator in the resin decreased, the amount of photogenerated radicals at the threshold power would decrease in resins **R**<sup>5</sup>–**R**<sup>8</sup> and **R**<sup>1</sup>. Therefore, high threshold laser power would be obtained with low loading concentration of photoinitiator, which was in agreement with the data as shown in Table 3.

When the linear scanning speed increased from 10 to 1000  $\mu\text{m s}^{-1}$  for **R**<sup>1</sup>, the exposure time decreased from 40 to 0.4 ms and the threshold laser power increased from 0.64 to 2.53 mW. The components and polymerization threshold of **R**<sup>1</sup> were summarized in Table 4. The square of the threshold power increased with the decrease of the exposure time (Fig. 6). In this case, the  $E_{\text{th}}$  decreased from

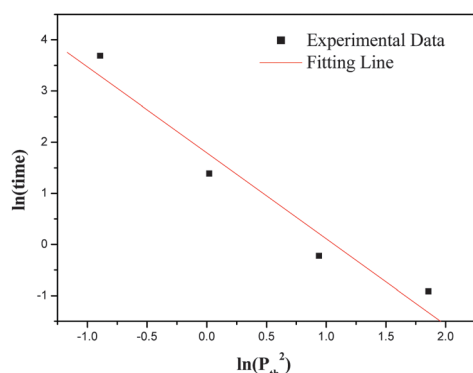


**Fig. 5** The dependence of threshold power on the concentration of photoinitiator **I**.

**Table 4** The dependence of threshold exposure intensity on scanning speed

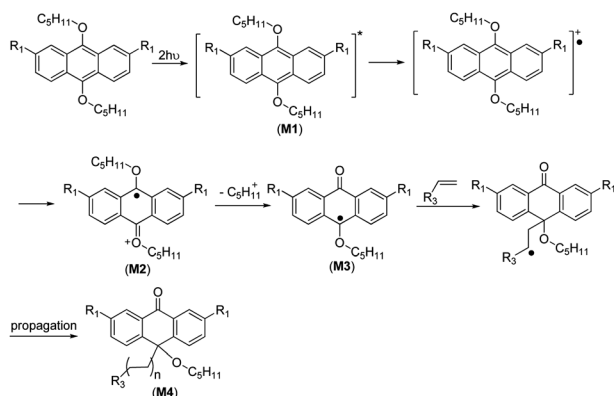
	MA (wt%)	DPE-6A (wt%)	MR <sup>a</sup> (%)	$\nu_s^b$ ( $\mu\text{m s}^{-1}$ )	$P_{\text{th}}^c$ (mW)	$E_{\text{th}}^d$ ( $\text{mJ cm}^{-2}$ )
<b>R<sup>I</sup></b>	66.47	32.59	0.18	10	0.64	$2.77 \times 10^7$
<b>R<sup>II</sup></b>	66.47	32.59	0.18	100	1.01	$4.37 \times 10^6$
<b>R<sup>I</sup></b>	66.47	32.59	0.18	500	1.60	$1.39 \times 10^6$
<b>R<sup>I</sup></b>	66.47	32.59	0.18	1000	2.53	$1.09 \times 10^6$

<sup>a</sup> Molar ratio of initiator in resin. <sup>b</sup> Linear scanning speed. <sup>c</sup> Threshold power of dye in resin. <sup>d</sup> Exposure intensity at threshold power.

**Fig. 6** The dependence of threshold power on the exposure time.

$2.77 \times 10^7 \text{ mJ cm}^{-2}$  to  $1.09 \times 10^6 \text{ mJ cm}^{-2}$ . The  $E_{\text{th}}$  value is obviously lower than that reported previously in reference 24. The results further indicate that **I** has extremely high sensitivity as TPIP initiator.

In order to clarify initiating efficiency difference of **I**, **II** and **III**, the TPIP initiating mechanism has been proposed based on the mechanism deduced from single-photon photoinitiating chemical studies as shown in Scheme 2.<sup>23</sup> When excited by a two-photon absorption process, anthracene derivatives absorb two photons to produce activated species **M1**. The species **M1** undergoes an electron photooxidation process to generate cationic radical species **M2** in the 9,10-position. Those with electron donor groups could effectively increase the reduction potential and stabilize the cationic radical **M2**. Then, the cationic radical **M2** undergoes a C–O cleavage to form a radical **M3** at 9,10-position. Consequently, the free radical

**Scheme 2** The mechanism of two-photon photoinitiated polymerization at 800 nm.

species **M3** initiate the polymerization of methyl acrylate derivatives. In our study, the stability of formed radicals is supposed to be **I** > **II** > **III** since the electron donating ability is **I** > **II** > **III**. The larger  $\delta_{\text{TPA}}$  at 800 nm and the stronger electron donating ability of dimethylamino group in **I** compared with methyl group in **II** and cyano group in **III** contribute to the higher sensitivity of **I**. Therefore, higher sensitivity and more rapid polymerization speed were observed when **I** was used as TPIP initiator.

## 4. Conclusions

In summary, we have designed and synthesized a series of new  $C_{2v}$  symmetrical 2,7-bis[2-(4-substituted phenyl)-vinyl]-9,10-dipenthyloxyanthracenes (**I**, **II** and **III**) by Wittig reaction as TPIP photoinitiators. **I** possesses a relatively lower fluorescence quantum yield, a larger two-photon absorption cross section and higher two-photon polymerization initiating efficiency compared with **II** and **III** in the range of 700–850 nm. In TPIP experiments, low thresholds of 0.64 mW and 2.53 mW have been achieved with 0.18% molar ratio loading of **I** in resin at the scanning speed of  $10 \mu\text{m s}^{-1}$  and  $1000 \mu\text{m s}^{-1}$ , respectively. When the molar ratio loading of **I** decreased to 0.01% in resin, the threshold increased to 5.06 mW. The high TPIP photoinitiating sensitivity of **I** was attributed to the  $C_{2v}$  symmetrical structure, dialkoxyanthracene core and strong electron donating ability of dimethylamino group. The stability of formed radicals is supposed to be **I** > **II** > **III** since the electron donating ability is **I** > **II** > **III**. Therefore, the photoinitiator efficiency followed a simple electron-donating effect trend (**I** > **II** > **III**).

## Acknowledgements

We are grateful for 973 (2010CB934103), ICP programs of MOST (2010DFA01180), the National Natural Science Foundation of China (Grant No. 50973126, 60907019, 61077028, 91123032), and Japan Science and Technology Agency (JST).

## Notes and references

- S. Kawata, H. B. Sun, T. Tanaka and K. Takada, *Nature*, 2001, **412**, 697–698; D. F. Tan, Y. Li, F. J. Qi, H. Yang, Q. H. Gong, X. Z. Dong and X. M. Duan, *Appl. Phys. Lett.*, 2007, **90**, 071106; X. Z. Dong, Z. S. Zhao and X. M. Duan, *Appl. Phys. Lett.*, 2008, **92**, 091113; M. Pawlicki, H. A. Collins, R. G. Denning and H. L. Anderson, *Angew. Chem., Int. Ed.*, 2009, **48**, 3244–3266; J. E. Koskela, S. Turunen, L. Yla-Outinen, S. Narkilahti and M. Kellomaki, *Polym. Adv. Technol.*, 2011, **23**, 992–1001; Y. Y. Cao, N. Takeyasu, T. Tanaka, X. M. Duan and S. Kawata, *Small*, 2009, **5**, 1144–1148.
- W. H. Zhou, S. M. Kuebler, K. L. Braun, T. Y. Yu, J. K. Cammack, C. K. Ober, J. W. Perry and S. R. Marder, *Science*, 2002, **296**, 1106–1109; T. Watanabe, M. Akiyama, K. Totani, S. M. Kuebler, F. Stellacci, W. Wenseleers, K. Braun, S. R. Marder and J. W. Perry, *Adv. Funct. Mater.*, 2002, **12**, 611–614; K. Kaneko, H. B. Sun, X. M. Duan and S. Kawata, *Appl. Phys. Lett.*, 2003, **83**, 2091–2093; C. N. LaFratta, J. T. Fourkas, T. Baldacchini and R. A. Farrer, *Angew. Chem., Int. Ed.*, 2007, **46**, 6238–6258; X. Z. Dong, Z. S. Zhao and X. M. Duan, *Appl. Phys. Lett.*, 2007, **91**, 124103; X. Z. Dong, Q. Ya, X. Z. Sheng, Z. Y. Li, Z. S. Zhao and X. M. Duan, *Appl. Phys. Lett.*, 2008, **92**, 231103; Z. B. Sun, X. Z. Dong, W. Q. Chen, S. Shoji, X. M. Duan and S. Kawata, *Adv. Mater.*, 2008, **20**,

- 914–919; W. K. Wang, Z. B. Sun, M. L. Zheng, X. Z. Dong, Z. S. Zhao and X. M. Duan, *J. Phys. Chem. C*, 2011, **115**, 11275–11281; X. M. Duan, H. B. Sun, K. Kaneko and S. Kawata, *Thin Solid Films*, 2004, **453–454**, 518–521.
- 3 K. J. Schafer, J. M. Hales, M. Balu, K. D. Belfield, E. W. Van Stryland and D. J. Hagan, *J. Photochem. Photobiol., A*, 2004, **162**, 497–502.
- 4 S. M. Kuebler, K. L. Braun, W. H. Zhou, J. K. Cammack, T. Yu, C. K. Ober, S. R. Marder and J. W. Perry, *J. Photochem. Photobiol., A*, 2003, **158**, 163–170; Y. M. Lu, F. Hasegawa, S. Ohkuma, T. Goto, S. Fukuhara, Y. Kawazu, K. Totani, T. Yamashita and T. Watanabe, *J. Mater. Chem.*, 2004, **14**, 1391–1395; J. Gu, W. Yulan, W. Q. Chen, X. Z. Dong, X. M. Duan and S. Kawata, *New J. Chem.*, 2007, **31**, 63–68; X. M. Wang, F. Jin, Z. G. Chen, S. Q. Liu, X. H. Wang, X. M. Duan, X. T. Tao and M. H. Jiang, *J. Phys. Chem. C*, 2011, **115**, 776–784; X. M. Wang, F. Jin, W. Z. Zhang, X. T. Tao, X. M. Duan and M. H. Jiang, *Dyes Pigment.*, 2011, **88**, 57–64.
- 5 E. Zojer, D. Beljonne, P. Pacher and J. L. Brédas, *Chem.–Eur. J.*, 2004, **10**, 2668–2680; G. S. He, L. S. Tan, Q. Zheng and P. N. Prasad, *Chem. Rev.*, 2008, **108**, 1245–1330; H. C. Zhang, E. Q. Guo, Y. L. Zhang, P. H. Ren and W. J. Yang, *Chem. Mater.*, 2009, **21**, 5125–5135; F. Todescato, I. Fortunati, S. Carlotto, C. Ferrante, L. Grisanti, C. Sissa, A. Painelli, A. Colombo, C. Dragonetti and D. Roberto, *Phys. Chem. Chem. Phys.*, 2011, **13**, 11099–11109; E. Collini, *Phys. Chem. Chem. Phys.*, 2012, **14**, 3725–3736.
- 6 K. D. Belfield, X. Ren, E. W. Van Stryland, D. J. Hagan, V. Dubikovskiy and E. J. Miesak, *J. Am. Chem. Soc.*, 2000, **122**, 1217–1218; P. J. Campagnola, D. M. Delguidice, G. A. Epling, K. D. Hoffacker, A. R. Howell, J. D. Pitts and S. L. Goodman, *Macromolecules*, 2000, **33**, 1511–1513; C. Li, L. Luo, S. Wang, W. Huang, Q. Gong, Y. Yang and S. Feng, *Chem. Phys. Lett.*, 2001, **340**, 444–448.
- 7 E. W. Nelson, T. P. Carter and A. B. Scranton, *Macromolecules*, 1994, **27**, 1013–1019; K. Tanaka, Y. Koizumi, T. Igarashi and T. Sakurai, *Macromolecules*, 2006, **39**, 8556–8558.
- 8 W. J. Yang, D. Kim, M. Y. Jeong, H. Kim, S. J. Jeon and B. R. Cho, *Chem. Commun.*, 2003, 2618–2619; W. J. Yang, C. H. Kim, M. Y. Jeong, S. K. Lee, M. J. Piao, S. J. Jeon and B. R. Cho, *Chem. Mater.*, 2004, **16**, 2783–2789; S. Kim, Q. D. Zheng, G. S. He, D. J. Bharali, H. E. Pudavar, A. Baev and P. N. Prasad, *Adv. Funct. Mater.*, 2006, **16**, 2317–2323; W. J. Yang, M. S. Seo, X. Q. Wang, S. J. Jeon and B. R. Cho, *J. Fluoresc.*, 2008, **18**, 403–411; Y. L. Zhang, P. H. Ren, H. C. Zhang, E. Q. Guo and W. J. Yang, *J. Fluoresc.*, 2010, **130**, 527–530.
- 9 W. J. Yang, D. Kim, M. Y. Jeong, H. Kim, Y. Lee, X. Fang, S. J. Jeon and B. R. Cho, *Chem.–Eur. J.*, 2005, **11**, 4191–4191.
- 10 J. F. Xing, W. Q. Chen, X. Z. Dong, T. Tanaka, X. Y. Fang, X. M. Duan and S. Kawata, *J. Photochem. Photobiol., A*, 2007, **189**, 398–404; W. E. Lu, X. Z. Dong, W. Q. Chen, Z. S. Zhao and X. M. Duan, *J. Mater. Chem.*, 2011, **21**, 5650–5659.
- 11 G. Jones, W. R. Jackson, C. Y. Chou and W. R. Bergmark, *J. Phys. Chem.*, 1985, **89**, 294–300.
- 12 C. Xu and W. W. Webb, *J. Opt. Soc. Am. B*, 1996, **13**, 481–491.
- 13 G. T. Morgan and E. A. Coulson, *J. Chem. Soc.*, 1929, 2551.
- 14 J. Brunel, O. Mongin, A. Jutand, I. Ledoux, J. Zyss and M. Blanchard-Desce, *Chem. Mater.*, 2003, **15**, 4139–4148.
- 15 S. K. Lee, W. J. Yang, J. J. Choi, C. H. Kim, S. J. Jeon and B. R. Cho, *Org. Lett.*, 2005, **7**, 323–326.
- 16 K. D. Belfield, A. R. Morales, B. S. Kang, J. M. Hales, D. J. Hagan, E. W. Van Stryland, V. M. Chapela and J. Percino, *Chem. Mater.*, 2004, **16**, 4634–4641.
- 17 J. P. Malval, F. Morlet-Savary, H. Chaumeil, L. Balan, D. L. Versace, M. Jin and A. Defoin, *J. Phys. Chem. C*, 2009, **113**, 20812–20821.
- 18 C. Toro, L. De Boni, S. Yao, K. D. Belfield and F. E. Hernandez, *J. Phys. Chem. B*, 2008, **112**, 12185–12190.
- 19 C. A. Zoto and R. E. Connors, *J. Mol. Struct.*, 2010, **982**, 121–126.
- 20 K. D. Belfield, K. J. Schafer, Y. Liu, J. Liu, X. Ren and E. W. Van Stryland, *J. Phys. Org. Chem.*, 2000, **13**, 837–849; S. Ohira, I. Rudra, K. Schmidt, S. Barlow, S. J. Chung, Q. Zhang, J. Matichak, S. R. Marder and J. L. Brédas, *Chem.–Eur. J.*, 2008, **14**, 11082–11091.
- 21 Y. Ren, X. Q. Yu, D. J. Zhang, D. Wang, M. L. Zhang, G. B. Xu, X. Zhao, Y. P. Tian, Z. S. Shao and M. H. Jiang, *J. Mater. Chem.*, 2002, **12**, 3431–3437.
- 22 J. F. Xing, X. Z. Dong, W. Q. Chen, X. M. Duan, N. Takeyasu, T. Tanaka and S. Kawata, *Appl. Phys. Lett.*, 2007, **90**, 131106.
- 23 J. V. Crivello and W. Jang, *J. Photochem. Photobiol., A*, 2003, **159**, 173–188.
- 24 J. F. Xing, W. Q. Chen, J. Gu, X. Z. Dong, N. Takeyasu, T. Tanaka, X. M. Duan and S. Kawata, *J. Mater. Chem.*, 2007, **17**, 1433–1438.